APL Photonics

Invited Article: Time-bin entangled photon pairs from Bragg-reflection waveguides

Cite as: APL Photonics 3, 080804 (2018); https://doi.org/10.1063/1.5038186
Submitted: 02 May 2018 • Accepted: 04 July 2018 • Published Online: 01 August 2018

H. Chen, S. Auchter, M. Prilmüller, et al.

Invited Article: Time-bin entangled photon pairs from Bragg-reflection waveguides

H. Chen,[1,2] S. Auchter,[1] M. Prilmüller,[1] A. Schlager,[1] T. Kauten,[1] K. Laiho,[3] B. Pressl,[1] H. Suchomel,[4] M. Kamp,[4] S. Höfling,[4,5] C. Schneider,[4] and G. Weihs[1]

[1]*Institut für Experimentalphysik, Universität Innsbruck, Technikerstraße 25, 6020 Innsbruck, Austria*
[2]*Department of Physics, National University of Defense Technology, Changsha 410073, People's Republic of China*
[3]*Technische Universität Berlin, Institut für Festkörperphysik, Hardenbergstr. 36, 10623 Berlin, Germany*
[4]*Technische Physik, Universität Würzburg, Am Hubland, 97074 Würzburg, Germany*
[5]*School of Physics and Astronomy, University of St Andrews, St Andrews KY16 9SS, United Kingdom*

(Received 2 May 2018; accepted 4 July 2018; published online 1 August 2018)

Semiconductor Bragg-reflection waveguides are well-established sources of correlated photon pairs as well as promising candidates for building up integrated quantum optics devices. Here, we use such a source with optimized non-linearity for preparing time-bin entangled photons in the telecommunication wavelength range. By taking advantage of pulsed state preparation and efficient free-running single-photon detection, we drive our source at low pump powers, which results in a strong photon-pair correlation. The tomographic reconstruction of the state's density matrix reveals that our source exhibits a high degree of entanglement. We extract a concurrence of 88.9(1.8)% and a fidelity of 94.2(9)% with respect to a Bell state.
https://doi.org/10.1063/1.5038186

I. INTRODUCTION

Robust entangled photon sources are vital for performing quantum optics tasks fast and reliably. For example, in a variety of quantum communication applications, no matter whether performed on the ground or via a satellite,[1–4] integrated quantum resources can be very useful. If the entangled photon sources, which are often based on bulk crystals, are replaced with integrated optics, one does not only greatly save space and reach better scalability but also gains in optical stability.[5,6]

Semiconductors provide an interesting integrated optics platform for preparing photon pairs via nonlinear optical effects, such as parametric down-conversion (PDC).[7–9] By utilizing Bragg-reflection waveguides (BRWs) made of $Al_xGa_{1-x}As$ with x being the aluminum concentration, we can benefit from their large effective second-order optical nonlinearity[10] and the flexibility in their design.[11] Moreover, for constructing large-scale fiber-optic networks, these structures have a broad transparency window in the telecommunication wavelengths and they benefit from the electro-optic capability of $Al_xGa_{1-x}As$ so that both active and passive optical elements can be realized.[12–14] Well-established fabrication technologies are available, which render these monolithic structures altogether excellent for nonlinear integrated optics.

In order for the PDC process to occur, the interacting light modes need to fulfill energy and momentum conservation.[15–17] Recently, BRWs based on the interaction of fundamental and higher order spatial modes have become popular for generating collinearly propagating pairs of photons, usually called signal and idler,[9,18–20] and a lot of effort has been put into optimizing their performance. For example, BRWs with a very low birefringence have proven to be versatile sources of polarization entangled states.[21–24] Additionally, such semiconductor waveguides are good candidates for

producing photon pairs with electrical pumping, in other words, by integrating the pump laser with the PDC source on the same chip.[25,26]

Semiconductor waveguides have also been shown to emit time-energy entangled photons[27,28] that were first treated by Franson in 1989.[29] However, in order to achieve a high degree of entanglement, these realizations require a highly coherent pump laser. A more versatile variant, using a pulsed excitation scheme, is time-bin entanglement,[30] in which a photon pair is created into a coherent superposition of two subsequent time bins with a well-defined relative phase. The pulsed operation is convenient for performing quantum optics tasks fast, and when being transmitted over long distances in optical fibers, time-bin entangled photons are more robust against decoherence than the polarization-entangled ones due to the inevitable polarization-mode dispersion.[31]

In the past, these types of entanglement have been demonstrated on various quantum photonic platforms ranging from PDC in bulk crystals[32–34] and waveguides[35,36] and spontaneous four wave mixing (FWM) in silicon waveguides and optical fibers[37,38] to photon emission from quantum dots.[39,40] While the latter work only in a highly controlled environment, FWM sources suffer from low conversion and background suppression efficiencies. Moreover, bulk crystals cannot be efficiently miniaturized and the integration of active components, like lasers, on conventional PDC materials[41] is not as straightforward as in $Al_xGa_{1-x}As$.[42]

Here, we demonstrate time-bin entanglement from a BRW sample that has been optimized to possess a high optical nonlinearity in a design process that is discussed in detail in Ref. 11. By combining pulsed pumping with efficient and fast free-running photo-detection, our PDC emitter produces a strong photon-pair correlation[43] and a low level of noise. Thereafter, we employ state tomography to reconstruct the density matrix of the time-bin entangled state. We demonstrate that BRWs can meet the demand of producing these states with a high degree of entanglement. Finally, with the help of the achieved concurrence, we can validate the quality of the entangled state and predict that a violation of Bell's inequality is possible with our source.

II. BRW SAMPLE AND PHOTON-PAIR CHARACTERISTICS

In our experiments, we utilize a multicore BRW sample as described in Ref. 11. The 365 nm thick BRW core of $Al_{0.428}Ga_{0.572}As$ is surrounded by 398 nm thick inner matching layers of $Al_{0.2}Ga_{0.8}As$ below and above. Around this core region are 356 nm thick outer matching layers of $Al_{0.628}Ga_{0.372}As$ and 6/5 layers of $Al_{0.2}Ga_{0.8}As/Al_{0.628}Ga_{0.372}As$ having thicknesses of 127 nm/443 nm. The sample is designed in a way that the largest aluminum concentration can be achieved by summing up the two lower concentrations, which simplifies the wafer growth process done via molecular beam epitaxy. The used BRW sample is reactive-ion plasma etched to just above the core and has a length of 2 mm and a ridge width of 4 μm. Its degeneracy wavelength of 1534 nm was determined via second harmonic generation, which is the bright counterpart of the PDC process. The type-II PDC process occurs between cross-polarized total-internal reflection modes in the telecom range and the Bragg modes in the near infrared, which is a higher order spatial mode.

First, we explore the performance of our BRW by investigating the characteristics of the emitted photons. For this purpose, we use the experiment described in Fig. 1(a). A pulsed Ti:Sapphire laser (76.2 MHz repetition rate, 767 nm central wavelength, and 0.8 nm bandwidth) is used as a pump for the PDC process. A small fraction of the pump beam is sent to a fast photodiode via a beam sampler to generate an electronic trigger signal for synchronizing the measurement devices. Thereafter, the beam passes through a polarization control setup of a half-wave plate and a sheet polarizer and through a short pass filter. The pump beam is then coupled into the BRW with a 100× microscope objective, whereas the light coupled out of the BRW is collimated with an aspheric lens. A dichroic mirror separates the residual pump beam from the PDC emission, which is then sent through a spectral filter, which has a 12 nm bandwidth and is centered at the degeneracy wavelength. Filtering is used to limit the spectral range of the PDC emission and to suppress residual background illumination. A polarizing beam splitter separates the cross-polarized signal and idler beams, which are collected with aspheric lenses into single-mode fibers and detected with superconducting nanowire single-photon detectors (SNSPDs, SingleQuantum Eos), which are optimized for the telecom C-band and have detection efficiencies better than 60%. In our setup, their combined rates of measured background

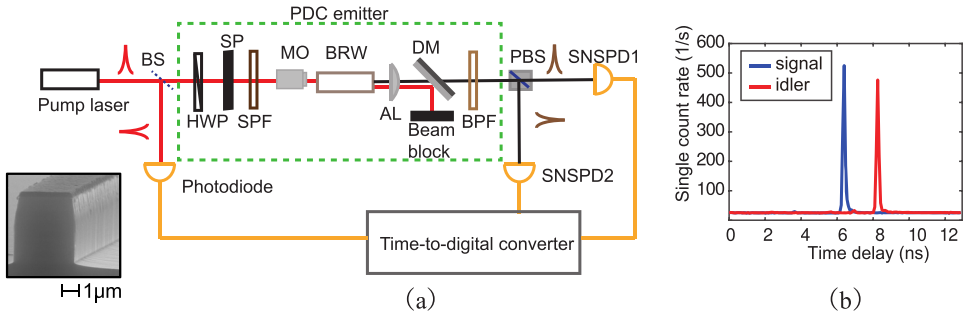

FIG. 1. (a) Measurement setup for investigating the properties of photon-pair emission from the BRW. The inset shows a scanning electron microscope image of a BRW facet. (b) Histograms of detection events in SNSPD1 and SNSPD2 with respect to the time elapsed from the detection of the laser trigger at the pump power of 60 μW. The two curves are shifted for better visibility. Abbreviations: AL: aspheric lens, BPF: band-pass filter, BS: beam sampler, DM: dichroic mirror, HWP: half-wave plate, SPF: short pass filter, MO: microscope objective, PBS: polarizing beam splitter, SNSPD: superconducting nanowire single-photon detector, SP: sheet polarizer.

light and dark counts are 360(60)/s for the signal channel and 390(80)/s for the idler channel. Finally, a time-to-digital converter is used to record time stamps of the detected photons and the laser trigger.

We start by investigating the single counts in signal and idler, shown in Fig. 1(b) for an average incident pump power of approximately 60 μW measured in front of the BRW before the microscope objective. Due to the pulsed pump, it is justified to apply time gatings of 0.5 ns at the detection. We achieve gated single count rates of 1210(40)/s and 1090(40)/s for signal and idler, respectively. The difference between the measured single counts in signal and idler is caused by the slightly different coupling efficiencies into the single-mode fibers connected to the two SNSPDs. From the signal-to-noise ratio (SNR) of the temporal traces of single counts in Fig. 1(b), we can ascertain that our BRW emits well-behaved pulsed PDC. We extract an SNR value as high as 20.8(9), which verifies the low level of total remaining background light. Moreover, the achieved coincidence count rate of 46(7)/s is almost perfectly free from spurious counts.

Next, we measure the single and coincidence counts as a function of pump power to characterize the photon-pair properties of the emitted PDC light. We evaluate the Klyshko efficiency[44] for signal (idler) as the ratio of coincidence counts to the single counts in idler (signal) with respect to the pump power as shown in Fig. 2(a). We see that at incident pump powers below about 10 μW, this ratio is limited by the background noise, which contributes to the gated single counts and lowers the Klyshko efficiency. Additionally, the Klyshko efficiency is expected to grow with increasing pump power due to the higher photon numbers in the PDC emission. Therefore, we exclude the apparent drop of the Klyshko efficiency at weak pumping from our linear fits, extrapolate them to low pump powers, and obtain the values of 4.12(9)% and 3.77(8)% for the total collection efficiencies of the signal and idler,

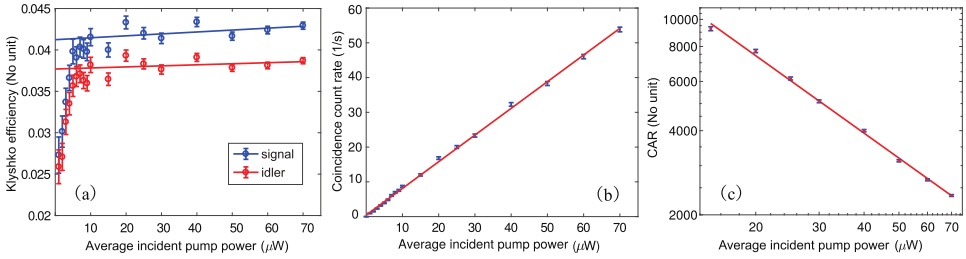

FIG. 2. (a) The Klyshko efficiency for signal and idler, (b) the coincidence count rate, and (c) the CAR with respect to the average incident pump power. At higher pump powers, the Klyshko efficiency seems to oscillate slightly, which is presumed to be related to Fabry-Perot effects in the BRW resulting from its well-cleaved and decently reflecting end facets. Symbols indicate the measured values, whereas the solid lines are fitted. The estimated error bars include statistical fluctuations only.

respectively. Moreover, we emphasize that this measurement sets a lower bound for the usable pump power to gain well-defined PDC emission.

The power dependence of the coincidence counts [Fig. 2(b)] shows the linear behavior of a spectrally multimodal PDC process and delivers the source brightness. The coincidence counts increase with a rate of 750(30) counts s^{-1} mW^{-1} with respect to the average incident pump power measured before the microscope objective. This figure of merit describes how well the pump light can be converted to detected pairs of photons. Thus, it is affected by all experimental light coupling and detection imperfections as well as the strength of the nonlinearity, the waveguide losses and spectral filtering. It is also affected by the confinement of modes and their interaction length. In our experiment, the rather high losses of the waveguide and the poor coupling of the pump light into the Bragg-mode each decrease the BRW's brightness by about an order of magnitude.[45] Additionally, we note that even though these factors are limiting the performance of our BRW, other waveguide designs on AlGaAs have reached lower propagation losses,[46,47] and shaping the spatial mode of the pump to better match with the Bragg-mode can help increase the total brightness.[21,25,26] When corrected for these effects, the achieved brightness of our BRW compares well to the conventional sources.[48]

Finally, we explore the coincidences-to-accidentals ratio (CAR), which is a loss-independent measure of the photon-pair correlation between the signal and idler. We estimate the CAR via R_C/R_A, in which R_C is the measured rate of coincidences and the accidental rate is estimated via $R_A = R_s R_i / R_t$, where R_s is the measured rate of singles in the signal output, R_i that of the idler (i), and R_t is the trigger rate. In Fig. 2(c), we present the CAR for our BRW with respect to the average incident pump power in the region where the PDC emission dominates over any background [see Fig. 2(a)] and achieve a CAR as high as 9260(150). Investigating the CAR on a logarithmic scale reveals whether the power dependencies of the single and coincidence counts deviate from each other. Assuming that $R_{s,i,C} \propto P$, with P being the pump power, we expect to find a slope of −1. Instead we find −0.918(15) which indicates minor imperfections in the photon-pair process and its detection. Nevertheless, the achieved values indicate a strong photon-number correlation between the signal and idler.

III. PREPARATION AND CHARACTERIZATION OF TIME-BIN ENTANGLED STATES

In order to prepare and detect time-bin entangled states, we extend our setup in Fig. 1(a) and use the setup depicted in Fig. 3(a). Before coupling the pump laser with its incident power of 100 μW to our BRW, we employ an imbalanced Mach-Zehnder interferometer to transform the pulsed pump into a coherent superposition of two pulses that define the so-called "early" and "late" time bins. The time delay between these pulses is about 3 ns, which is much shorter than the time of 13.1 ns between two successive pump laser pulses. Additionally, before detection, we send the signal and idler through similar interferometers having the same delay between the "early" and "late" time bins as the pump interferometer. In the experiment, the three interferometers are combined in a single

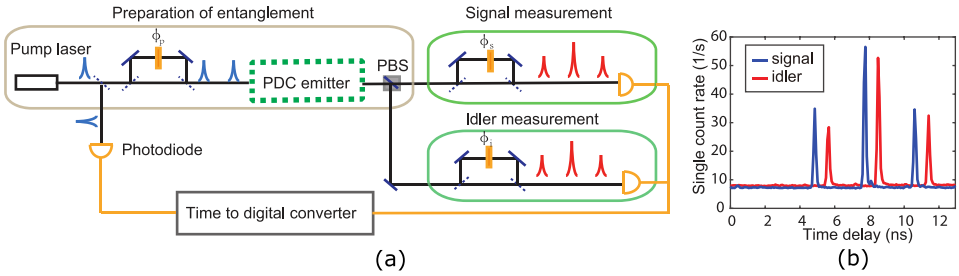

FIG. 3. (a) Measurement setup for generating and detecting time-bin entanglement using the PDC emitter from Fig. 1. (b) Histograms of the detection events in SNSPD1 and SNSPD2 with respect to the time elapsed from the detection of the laser trigger at an incident pump power of 100 μW. The unbalanced Mach-Zehnder interferometers are used for the entanglement generation and detection. The phase of each interferometer (ϕ_p, ϕ_s, ϕ_i) is controlled by rotating glass plates on motorized stages placed in the long arms of the interferometers.

multi-path free-space setup similar to the one reported in Ref. 39. For measuring the interference fringe patterns, we integrate over 2 min at each setting, while we increase this integration time to 20 min for doing the state tomography in order to grow the ensemble size and statistical accuracy. Active stabilization realized with a reference beam can help compensate long term phase drifts in all three distinct spatial modes. For this purpose, a fiber-coupled and frequency stabilized He-Ne laser is sent into the interferometer and detected with a fast photo-diode at one of its output ports. In order to keep the path length difference constant, a piezo-mounted retro-reflector is adjusted according to its reading.

For achieving a maximally entangled state, we require that the "early" and "late" pump pulses generate photon pairs with the same probability. Additionally, the probability to generate two photon pairs, one in the "early" pump pulse and another in the "late" pump pulse, has to be negligible. If these conditions are met, the photon pairs are emitted in the time-bin entangled state

$$|\Phi\rangle = \frac{1}{\sqrt{2}}(|0\rangle_s|0\rangle_i + e^{i\phi_p}|1\rangle_s|1\rangle_i), \tag{1}$$

in which $|0\rangle$ and $|1\rangle$ denote the early and late states and the variable ϕ_p is the pump interferometer's phase.

Figure 3(b) illustrates histograms of the detected single count events for both the signal and idler. We can clearly see three distinct peaks. The leftmost peak corresponds those events, in which the signal and idler photons are created by the early pump pulse and they both pass through the short paths of the detection interferometers. Similarly, in the case of the rightmost events, the pump and PDC photons traverse the long paths of the interferometers. The central peaks are nearly twice as high as the surrounding ones, since the photons created by the early-pump and traveling through long paths of the signal and idler interferometers accumulate with those generated from the late-pump and passing through the short paths. Additionally, since photon pairs produced from an "early-pump/long-analysis-path" case are indistinguishable from the "late-pump/short-analysis-path" case, the cross correlation of the central peaks of the signal and idler shows interference fringes, depending on the relative phase of the output interferometers.

In Fig. 4, we illustrate this interference by presenting the signal and idler coincidences within the five possible discrete time delays between their detections for two cases that result in the maximal and minimal amounts of measured coincidences, respectively. Again, we employ time gates of 0.5 ns width to separate the coincidence peaks from each other. The rate of coincidences R in the central peak oscillates sinusoidally with respect to the phase change in the pump, signal, and idler interferometers and is given by[49]

$$R \propto 1 - V\cos(\phi_s + \phi_i - \phi_p), \tag{2}$$

in which ϕ_s and ϕ_i are the phases of the signal and idler interferometer, respectively, and V denotes the fringe visibility. While the visibility in the time basis is typically almost perfect, we emphasize that V is a measure of the quality of the interference when the state is projected into a superposition of the time bins. Therefore, it is often degraded due to the state's impurity.

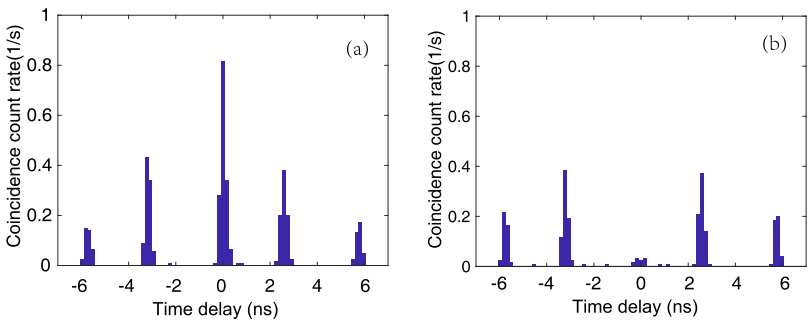

FIG. 4. Interferograms of coincidences between the signal and idler shown in Fig. 3(b) with respect to the time delay between their detection at two relative signal and idler interferometers' phases resulting in (a) maximal and (b) minimal amount of coincidences.

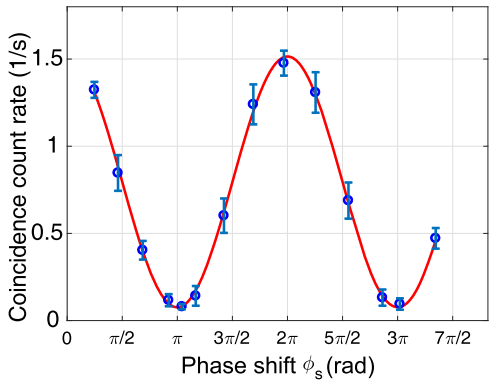

FIG. 5. Measured coincidence count rates (symbols) with respect to the phase change in the signal interferometer. The solid line represents a sinusoidal fit.

Figure 5 shows the measured coincidence count rate in the central peak with respect to the phase in the signal interferometer including the data in Fig. 4. This phase can be changed by rotating the glass plates placed in the long arms of the interferometers. We observe a fringe visibility of 90.7(1.6)% without any compensation of accidental counts or subtraction of other background contributions. We attribute the slight degradation in the visibility to minor imperfections in the mode overlap of the used interferometer. The effect of spurious counts on the visibility can be estimated via the CAR, which was in the measurement 740(30). If just the finite CARs were responsible, the highest achievable visibility would be 99.73(1)%, which is well-above our experimental value.

To fully characterize the prepared entangled state from Fig. 5, we perform a tomographic reconstruction of the density matrix by projecting the prepared state onto four different bases, which we define as $|0\rangle$, $|1\rangle$, $|+X\rangle = \frac{|0\rangle+|1\rangle}{2}$, and $|+Y\rangle = \frac{|0\rangle+i|1\rangle}{\sqrt{2}}$. By performing 16 correlation measurements between all combinations of $\{|0\rangle, |1\rangle, |+X\rangle, |+Y\rangle\}$, we reconstruct the 4×4 density matrix of our time-bin entangled state. For this purpose, we only need four different measurements with the signal and idler interferometers' phases (ϕ_s, ϕ_i) set to the values of (0°, 0°), (0°, 90°) and (90°, 90°), (90°, 0°), which reveal the visibilities in the superposition bases with 0° corresponding to $|+X\rangle$ and 90° to $|+Y\rangle$, respectively.[50] The glass plates' angles are calibrated via the fringe pattern measurement. We assign the phases (0°, 0°) to angle settings at which a maximum amount of coincidences are expected in Fig. 5. By finding the coincidence minimum corresponding to the phases (0°, 180°), we can extract the angle settings required for the state tomography.

Finally, we reconstruct the density matrix using the maximum likelihood method described in Refs. 51 and 52. The errors are recovered via Monte-Carlo simulations. The absolute values of the elements of the reconstructed density matrix ρ are given by

$$\mathrm{abs}(\rho) = \frac{1}{100}\cdot\begin{bmatrix} 50.9(8) & 1.7(7) & 1.8(7) & 44.5(9) \\ 1.7(7) & 0.3(1) & 0.17(7) & 2.5(7) \\ 1.8(7) & 0.17(7) & 0.21(9) & 1.4(7) \\ 44.5(9) & 2.5(7) & 1.4(7) & 48.6(8) \end{bmatrix}, \tag{3}$$

and its real and imaginary parts are shown in Fig. 6. The obtained density matrix includes, as expected, four main contributions and only a very small undesired background. The weights of the diagonal elements reflect the division of the power in the pump beam interferometer, and the main off-diagonal elements are mainly real valued as expected from Fig. 5.

From the density matrix in Fig. 3 we obtain a concurrence of 88.9(1.8)% and a fidelity of 94.1(5)% with respect to the state $|\Phi^+\rangle = \frac{1}{\sqrt{2}}(|0\rangle_s|0\rangle_i + |1\rangle_s|1\rangle_i)$. As the former quantifies the high degree of the entanglement achieved, the latter describes the probability of producing the target state $|\Phi^+\rangle$. Moreover, the obtained concurrence is greater than $1/\sqrt{2}$ and thus in principle high enough for violating Bell's inequality. Following Ref. 53, we can estimate the range of possible violations of the Clauser-Horne-Shimony-Holt (CHSH) inequality[54] for optimized measurement settings solely from the concurrence C as $[2\sqrt{1+C^2}, 2\sqrt{2}C] = 2.51(5)$ to $2.68(5)$. The lower and upper bounds

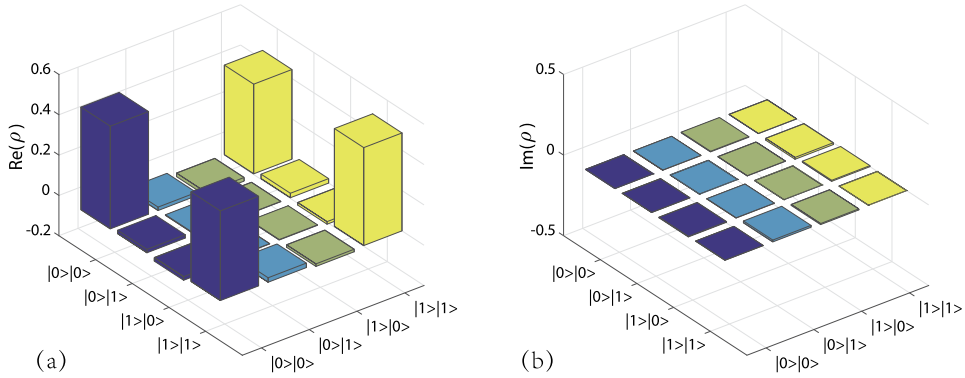

FIG. 6. (a) Real and (b) imaginary parts of the reconstructed density matrix given in Eq. (3).

are saturated by states with the lowest possible purity at the given concurrence and pure states, respectively. This highlights the suitability of BRWs as low noise PDC emitters for entangled state generation.

IV. CONCLUSION

Integrated optics devices provide means for miniaturizing the bulk optics components that are still today largely used in many quantum optics tasks. BRWs based on semiconductor materials are indeed good candidates to become truly practical as integrated quantum photonic components. We used a BRW sample with a simplified epitaxial structure designed for having a larger nonlinearity and for simplifying the fabrication process to produce cross-polarized signal and idler beams via PDC. By utilizing efficient, free-running single photon detectors, we can drive our source at low pump powers, enabling a modest Klyshko efficiency and a strong photon-pair correlation. Additionally, the power dependency of the CAR indicates only a small number of detected spurious counts. We prepared time-bin entangled states from the PDC emission of our BRW and achieved a high degree of entanglement without subtracting any spurious counts. We obtained a concurrence of 88.9(1.8)%, which is high enough to violate Bell's inequality and a fidelity of 94.2(0.9)% to the $|\Phi^+\rangle$ state. Our results offer means to develop BRWs that reach the low level of background noise required for the preparation of high quality entangled states from photon pairs. Additionally, we believe that further integration and miniaturization of our PDC emitter and the bulky interferometers will result in higher brightness and in better overlap of the modes required for achieving a higher concurrence. Altogether, our investigations pave the way for utilizing BRWs as robust sources of highly entangled photon pairs in the telecommunication wavelength range in pulsed operation.

ACKNOWLEDGMENTS

This work was supported by the Austrian Science Fund (FWF) through the Project Nos. I 2065 and J 4125, the DFG Project No. SCHN1376/2-1, the ERC project *EnSeNa* (No. 257531), the State of Bavaria, and the China Scholarship Council (No. 201503170272). We thank A. Wolf and S. Kuhn for assistance during sample growth and fabrication and J. Loitzl for laboratory assistance.

[1] T. Rudolph, "Why I am optimistic about the silicon-photonic route to quantum computing," APL Photonics **2**, 030901 (2017).
[2] X.-S. Ma, T. Herbst, T. Scheidl, D. Wang, S. Kropatschek, W. Naylor, B. Wittmann, A. Mech, J. Kofler, E. Anisimova, V. Makarov, T. Jennewein, R. Ursin, and A. Zeilinger, "Quantum teleportation over 143 kilometres using active feed-forward," Nature **489**, 269 (2012).
[3] J. Yin, Y. Cao, Y. H. Li, S. K. Liao, L. Zhang, J. G. Ren, W. Q. Cai, W. Y. Liu, B. Li, and H. Dai, "Satellite-based entanglement distribution over 1200 kilometers," Science **356**, 1140 (2017).
[4] K. Günthner, I. Khan, D. Elser, B. Stiller, O. Bayraktar, C. R. Müller, K. Sauke, D. Tröndle, F. Heine, S. Seel, P. Greulich, H. Zech, B. Gütlich, I. Richter, M. Lutzer, S. Philipp-May, R. Meyer, C. Marquardt, and G. Leuchs, "Quantum-limited measurements of optical signals from a geostationary satellite," Optica **4**, 611 (2017).

[5] J. L. O'Brien, "Optical quantum computing," Science **318**, 1567 (2007).
[6] A. Politi, M. J. Cryan, J. G. Rarity, S. Yu, and J. L. O'Brien, "Silica-on-silicon waveguide quantum circuits," Science **320**, 646 (2008).
[7] L. Lanco, S. Ducci, J.-P. Likforman, X. Marcadet, J. van Houwelingen, H. Zbinden, G. Leo, and V. Berger, "Semiconductor waveguide source of counterpropagating twin photons," Phys. Rev. Lett. **97**, 173901 (2006).
[8] P. Sarrafi, E. Y. Zhu, K. Dolgaleva, B. M. Holmes, D. C. Hutchings, J. S. Aitchison, and L. Qian, "Continuous-wave quasi-phase-matched waveguide correlated photon pair source on a III-V chip," Appl. Phys. Lett. **103**, 251115 (2013).
[9] R. Horn, P. Abolghasem, B. J. Bijlani, D. Kang, A. S. Helmy, and G. Weihs, "Monolithic source of photon pairs," Phys. Rev. Lett. **108**, 153605 (2012).
[10] R. W. Boyd, *Nonlinear Optics* (Academic Press, 2003).
[11] B. Pressl, K. Laiho, H. Chen, T. Günthner, A. Schlager, S. Auchter, H. Suchomel, M. Kamp, S. Höfling, C. Schneider, and G. Weihs, "Semi-automatic engineering and tailoring of high-efficiency Bragg-reflection waveguide samples for quantum photonic applications," Quantum Sci. Technol. **3**, 024002 (2017).
[12] S. Adachi, in *Properties of Aluminium Gallium Arsenide*, edited by S. Adachi (Inspec, London, 1993), No. 7.
[13] S. Gehrsitz, F. Reinhart, C. Gourgon, N. Herres, A. Vonlanthen, and H. Sigg, "The refractive index of $Al_xGa_{1-x}As$ below the band gap: Accurate determination and empirical modeling," J. Appl. Phys. **87**, 7825 (2000).
[14] C. P. Dietrich, A. Fiore, M. G. Thompson, M. Kamp, and S. Höfling, "GaAs integrated quantum photonics: Towards compact and multi-functional quantum photonic integrated circuits," Laser Photonics Rev. **10**, 870 (2016).
[15] B. R. West and A. S. Helmy, "Analysis and design equations for phase matching using Bragg reflector waveguides," IEEE J. Sel. Top. Quantum Electron. **12**, 431 (2006).
[16] A. S. Helmy, "Phase matching using Bragg reflection waveguides for monolithic nonlinear optics applications," Opt. Express **14**, 1243 (2006).
[17] A. S. Helmy, P. Abolghasem, J. Stewart Aitchison, B. J. Bijlani, J. Han, B. M. Holmes, D. C. Hutchings, U. Younis, and S. J. Wagner, "Recent advances in phase matching of second-order nonlinearities in monolithic semiconductor waveguides," Laser Photonics Rev. **5**, 272 (2011).
[18] T. Günthner, B. Pressl, K. Laiho, J. Geßler, S. Höfling, M. Kamp, C. Schneider, and G. Weihs, "Broadband indistinguishability from bright parametric downconversion in a semiconductor waveguide," J. Opt. **17**, 125201 (2015).
[19] C. Autebert, J. Trapateau, A. Orieux, A. Lemaître, C. Gomez-Carbonell, E. Diamanti, I. Zaquine, and S. Ducci, "Multi-user quantum key distribution with entangled photons from an AlGaAs chip," Quantum Sci. Technol. **1**, 01LT02 (2016).
[20] D. Kang, A. Anirban, and A. S. Helmy, "Monolithic semiconductor chips as a source for broadband wavelength-multiplexed polarization entangled photons," Opt. Express **24**, 15160 (2016).
[21] A. Vallés, M. Hendrych, J. Svozilík, R. Machulka, P. Abolghasem, D. Kang, B. J. Bijlani, A. S. Helmy, and J. P. Torres, "Generation of polarization-entangled photon pairs in a Bragg reflection waveguide," Opt. Express **21**, 10841 (2013).
[22] R. T. Horn, P. Kolenderski, D. Kang, P. Abolghasem, C. Scarcella, A. Della Frera, A. Tosi, L. G. Helt, S. V. Zhukovsky, J. E. Sipe *et al.*, "Inherent polarization entanglement generated from a monolithic semiconductor chip," Sci. Rep. **3**, 2314 (2013).
[23] A. Schlager, B. Pressl, K. Laiho, H. Suchomel, M. Kamp, S. Höfling, C. Schneider, and G. Weihs, "Temporally versatile polarization entanglement from Bragg reflection waveguides," Opt. Lett. **42**, 2102 (2017).
[24] D. Kang, M. Kim, H. He, and A. S. Helmy, "Two polarization-entangled sources from the same semiconductor chip," Phys. Rev. A **92**, 013821 (2015).
[25] B. J. Bijlani, P. Abolghasem, and A. S. Helmy, "Semiconductor optical parametric generators in isotropic semiconductor diode lasers," Appl. Phys. Lett. **103**, 091103 (2013).
[26] F. Boitier, A. Orieux, C. Autebert, A. Lemaître, E. Galopin, C. Manquest, C. Sirtori, I. Favero, G. Leo, and S. Ducci, "Electrically injected photon-pair source at room temperature," Phys. Rev. Lett. **112**, 183901 (2014).
[27] P. Sarrafi, E. Y. Zhu, B. M. Holmes, D. C. Hutchings, S. Aitchison, and L. Qian, "High-visibility two-photon interference of frequency–time entangled photons generated in a quasi-phase-matched AlGaAs waveguide," Opt. Lett. **39**, 5188 (2014).
[28] C. Autebert, N. Bruno, A. Martin, A. Lemaitre, C. G. Carbonell, I. Favero, G. Leo, H. Zbinden, and S. Ducci, "Integrated AlGaAs source of highly indistinguishable and energy-time entangled photons," Optica **3**, 143 (2016).
[29] J. D. Franson, "Bell inequality for position and time," Phys. Rev. Lett. **62**, 2205 (1989).
[30] J. Brendel, N. Gisin, W. Tittel, and H. Zbinden, "Pulsed energy-time entangled twin-photon source for quantum communication," Phys. Rev. Lett. **82**, 2594 (1999).
[31] J. Dynes, H. Takesue, Z. Yuan, A. Sharpe, K. Harada, T. Honjo, H. Kamada, O. Tadanaga, Y. Nishida, M. Asobe *et al.*, "Efficient entanglement distribution over 200 kilometers," Opt. Express **17**, 11440 (2009).
[32] I. Marcikic, H. de Riedmatten, W. Tittel, H. Zbinden, M. Legré, and N. Gisin, "Distribution of time-bin entangled qubits over 50 km of optical fiber," Phys. Rev. Lett. **93**, 180502 (2004).
[33] O. Kwon, K.-K. Park, Y.-S. Ra, Y.-S. Kim, and Y.-H. Kim, "Time-bin entangled photon pairs from spontaneous parametric down-conversion pumped by a cw multi-mode diode laser," Opt. Express **21**, 25492 (2013).
[34] F. Vedovato, C. Agnesi, M. Tomasin, M. Avesani, L. Jan-Åke, G. Vallone, and P. Villoresi, "Post-selection-loophole-free bell violation with genuine time-bin entanglement," e-print arXiv:1804.10150 (2018).
[35] S. Tanzilli, W. Tittel, H. De Riedmatten, H. Zbinden, P. Baldi, M. DeMicheli, D. B. Ostrowsky, and N. Gisin, "PPLN waveguide for quantum communication," Eur. Phys. J. D **18**, 155 (2002).
[36] L. Ma, O. Slattery, T. Chang, and X. Tang, "Non-degenerated sequential time-bin entanglement generation using periodically poled KTP waveguide," Opt. Express **17**, 15799 (2009).
[37] H. Takesue, N. Matsuda, E. Kuramochi, and M. Notomi, "Entangled photons from on-chip slow light," Sci. Rep. **4**, 3913 (2014).
[38] H. Takesue and K. Inoue, "Generation of 1.5-μm band time-bin entanglement using spontaneous fiber four-wave mixing and planar light-wave circuit interferometers," Phys. Rev. A **72**, 041804(R) (2005).

[39] H. Jayakumar, A. Predojević, T. Kauten, T. Huber, G. S. Solomon, and G. Weihs, "Time-bin entangled photons from a quantum dot," Nat. Commun. **5**, 4251 (2014).
[40] M. Prilmüller, T. Huber, M. Müller, P. Michler, G. Weihs, and A. Predojević, "Hyper-entanglement of photons emitted by a quantum dot," e-print arXiv:1701.08986 (2017).
[41] S. J. Herr, Y. Folwill, K. Buse, and I. Breunig, "Self-frequency doubling in a laser-active whispering-gallery resonator," Opt. Lett. **42**, 2627 (2017).
[42] T. W. Schlereth, C. Schneider, S. Gerhard, S. Höfling, and A. Forchel, "Short-wavelength (760–920 nm) AlGaInAs quantum dot lasers," IEEE J. Sel. Top. Quantum Electron. **15**, 792 (2009).
[43] M. Covi, B. Pressl, T. Günthner, K. Laiho, S. Krapick, C. Silberhorn, and G. Weihs, "Liquid-nitrogen cooled, free-running single-photon sensitive detector at telecommunication wavelengths," Appl. Phys. B **118**, 489 (2015).
[44] D. N. Klyshko, "Utilization of vacuum fluctuations as an optical brightness standard," Sov. J. Quantum Electron. **7**, 591 (1977).
[45] B. Pressl, T. Günthner, K. Laiho, J. Geßler, M. Kamp, S. Höfling, C. Schneider, and G. Weihs, "Mode-resolved Fabry-Perot experiment in low-loss Bragg-reflection waveguides," Opt. Express **23**, 33608 (2015).
[46] G. A. Porkolab, P. Apiratikul, B. Wang, S. H. Guo, and C. J. K. Richardson, "Low propagation loss AlGaAs waveguides fabricated with plasma-assisted photoresist reflow," Opt. Express **22**, 7733 (2014).
[47] L. Ottaviano, M. Pu, E. Semenova, and K. Yvind, "Low-loss high-confinement waveguides and microring resonators in AlGaAs-on-insulator," Opt. Lett. **41**, 3996 (2016).
[48] M. Fiorentino, S. M. Spillane, R. G. Beausoleil, T. D. Roberts, P. Battle, and M. W. Munro, "Spontaneous parametric down-conversion in periodically poled KTP waveguides and bulk crystals," Opt. Express **15**, 7479 (2007).
[49] I. Marcikic, H. de Riedmatten, W. Tittel, V. Scarani, H. Zbinden, and N. Gisin, "Time-bin entangled qubits for quantum communication created by femtosecond pulses," Phys. Rev. A **66**, 062308 (2002).
[50] H. Takesue and Y. Noguchi, "Implementation of quantum state tomography for time-bin entangled photon pairs," Opt. Express **17**, 10976 (2009).
[51] K. Banaszek, G. M. D'Ariano, M. G. A. Paris, and M. F. Sacchi, "Maximum-likelihood estimation of the density matrix," Phys. Rev. A **61**, 010304 (1999).
[52] J. B. Altepeter, E. R. Jeffrey, and P. G. Kwiat, "Photonic state tomography," Adv. At., Mol., Opt. Phys. **52**, 105 (2005).
[53] F. Verstraete and M. M. Wolf, "Entanglement versus Bell violations and their behavior under local filtering operations," Phys. Rev. Lett. **89**, 170401 (2002).
[54] J. F. Clauser, M. A. Horne, A. Shimony, and R. A. Holt, "Proposed experiment to test local hidden-variable theories," Phys. Rev. Lett. **23**(15), 880 (1969).